IEEE Access
Multidisciplinary ⋮ Rapid Review ⋮ Open Access Journal

Received 4 July 2023, accepted 18 July 2023, date of publication 24 July 2023, date of current version 1 August 2023.

Digital Object Identifier 10.1109/ACCESS.2023.3298206

RESEARCH ARTICLE

Decentralized Dynamic State Estimation of Transmission Lines Using Local Measurements

ANKUR SRIVASTAVA[1], (Member, IEEE), ABHINAV KUMAR SINGH[2], (Member, IEEE), LE ANH TUAN[3], (Member, IEEE), DAVID STEEN[3], (Member, IEEE), AND ABDUL SALEEM MIR[4], (Member, IEEE)

[1]Eversource Energy Center, University of Connecticut, Storrs, CT 06269, USA
[2]School of Electronics and Computer Science, University of Southampton, SO17 1BJ Southampton, U.K.
[3]Division of Electric Power Engineering, Department of Electrical Engineering, Chalmers University of Technology, 41296 Gothenburg, Sweden
[4]Department of Electrical Engineering, Indian Institute of Technology Roorkee, Roorkee 247667, India

Corresponding author: Ankur Srivastava (ankur.srivastava@uconn.edu)

This work was supported in part by the UNITED-GRID Project through the European Community's Horizon 2020 Framework Programme under Grant 773717, in part by the FlexiGrid Project through the European Community's Horizon 2020 Framework Programme under Grant 864048, and in part by the EPSRC U.K. Project EP/T021713/1.

ABSTRACT This paper presents a novel decentralized dynamic state estimation (DSE) method for estimating the dynamic states of a transmission line in real-time. The proposed method utilizes the sampled measurements from the local end of a transmission line, and thereafter DSE is performed by employing an unscented Kalman filter. The advantage of the proposed method is that the remote end state variables of a transmission line can be estimated using only the local end variables and, hence, the need for communication infrastructure is eliminated. Furthermore, an exact nonlinear model of the transmission line is utilized for estimation and the DSE of one transmission line is independent of the other lines. These in turn result in reduced complexity, higher accuracy, and easier implementation of the decentralized estimator. The proposed method is applied to a case study with realistic transmission line parameters. The results from the case study affirm that the proposed method accurately estimates the state variables under different operating conditions. Furthermore, robust performance is achieved with different noise variances and types. The proposed DSE method is envisioned to have potential applications in transmission line monitoring, control, and protection.

INDEX TERMS Dynamic state estimation, Kalman filter, power system monitoring, transmission line, unscented transformation.

I. INTRODUCTION

A. MOTIVATION

Climate change and global warming concerns have led to a transition from fossil fuel-based power generation to sustainable and environment-friendly renewables-based generation. Simultaneously, with the increase in electrification and load demand, the transmission system components are operated close to their operating limits. These changes (along with several other changes) pose the following main challenges related to the operation of the transmission systems [1], [2], [3]:

1) Renewable energy sources (RES) are characterized as stochastic, intermittent, non-synchronous, and power electronics interfaced. These characteristics make their operation and control more challenging, particularly, it is difficult to accurately track the system operating point.
2) Due to increasing RES penetration and electrification of different energy sectors, the prediction of power flow patterns in transmission systems is an uphill task as compared to centralized fossil fuel-based power generation.
3) The operation closer to the operating limit of components could stress the transmission systems which could also lead to partial power demand failure or blackouts.

Traditionally, the above-mentioned issues were handled using the control and monitoring tools available with the energy management systems (EMSs). However, such tools

The associate editor coordinating the review of this manuscript and approving it for publication was Fabio Mottola.

have become inadequate mainly due to the slow update rate of supervisory control and data acquisition (SCADA) systems within EMSs, and results based on steady-state models do not capture the fast system dynamics. The large-scale deployment of phasor measurement units (PMUs) in the last decades addressed some of the issues associated with fast capturing of system dynamics and the evaluation of online dynamic security assessment [4], [5]. Most of these works are based on DSE which is essential for time-critical operation, monitoring, and control of transitioning power systems [6].

At the same time, transmission lines, which are one of the important components in transmission systems, also require proper control and estimation mechanisms for real-time condition monitoring, fault location, and protection. DSE can be one of the potential solutions to meet such requirements. Proper metering infrastructure based on PMUs and merging units (MUs) is one of the main requirements in such applications [1]. The potential of DSE in the transmission line protection is explored in [2], [7], [8], [9], [10], [11], [12], [13], [14], [15], [16], and [17]. However, some of these works make grossly inaccurate approximations in both the modelling and the identification stages, because of which the speed and accuracy of transmission line estimation and protection are adversely affected. For instance, [2], [10], [11] use a quadratic approximation in the dynamic modelling, while for state estimation, the weighted least squares (WLS) method is employed in [10], [11], [12], and [13], an improved version of WLS in [8], unconstraint WLS method in [11], and Lagrangian multipliers in [2]. However, all these estimation methods are based on algorithms traditionally used in static state estimation (SSE) and, hence, do not adequately capture the system dynamics, as required by DSE. A cubature Kalman filter-based DSE method is employed in [16] for a wide-area backup protection scheme applied to line outage, generator outage, etc. An ensemble Kalman filter-based DSE method is presented in [18] which overcomes some of the limitations of WLS, however, it does not consider the second-order time derivative terms which leads to reduced estimation accuracy. The work presented in [14], advocates the use of unscented Kalman filter (UKF) with application to fault location for multi-terminal transmission lines. The transmission line model proposed in this study is nonlinear which is solved using the state estimation method. In addition to these limitations, the works related to DSE application in protection such as [2], [7], [8], [9], [15], and [17] require remote end measurements to perform DSE which clearly emphasizes the need for communication. Hence, these methods along with conventional protection schemes such as the differential, distance, and pilot relaying could maloperate in case of communication failures leading to misoperation.

B. CONTRIBUTIONS

An UKF-based decentralized DSE method has been proposed in this paper as a potential solution to the aforementioned challenges and limitations in transmission line DSE such as limited estimation accuracy, significant computational requirements, use of remote end measurements (emphasizing the need for communication infrastructure), etc. The proposed DSE method can estimate the state variables with improved estimation accuracy, low computational requirements, and using only local end measurements. The main advantages associated with the proposed method are as follows:

- This is the first work that performs decentralized DSE of transmission lines using only local measurements, and no other comparable work currently exists.
- Estimation has high accuracy and speed, as the estimation model does not require any approximations or linearizations, and the exact nonlinear dynamics of the transmission line are captured.
- Sampling requirements for DSE have been mathematically derived, without which decentralized DSE of transmission lines will fail to converge, or the estimation error will become too large.
- No communication infrastructure is required; thus, any communication failure, latency, packet loss, etc., will not impact the estimation quality.
- No inter-dependency between transmission lines as the estimation process for a transmission line is independent of the other line. This feature keeps any estimation errors remain segregated and thus makes them easier to identify.
- Estimation works with flat start or zero initial values. Hence, estimation accuracy does not depend on the accuracy of initialization.

The remainder of the paper is organized as follows. Section II explains the problem statement and the methodology used in the work. The transmission line modelling, unscented Kalman filter, pseudo inputs, and the choice of the sampling rate of DSE are presented in Section III. The details of the case study used in the work are given in Section IV. Section V presents and discusses the results of the case study. The evaluation of estimation performance under different conditions is done in Section VI. Finally, the conclusion is outlined in Section VII.

II. PROBLEM STATEMENT AND METHODOLOGY

With appropriate assumptions, the following time-continuous nonlinear differential and algebraic equations can be used to model a transmission line [19]:

$$\dot{\boldsymbol{x}}(t) = \bar{\boldsymbol{g}}[\dot{\boldsymbol{x}}(t), \boldsymbol{x}(t), \dot{\boldsymbol{u}}(t), \boldsymbol{u}(t), \boldsymbol{y}(t), \boldsymbol{v}(t)] \tag{1}$$

$$\boldsymbol{y}(t) = \boldsymbol{h}[\dot{\boldsymbol{x}}(t), \boldsymbol{x}(t), \dot{\boldsymbol{u}}(t), \boldsymbol{v}(t)] + \boldsymbol{w}(t) \tag{2}$$

The sampling of (1) and (2) at a sampling time period T_0 results in (3) and (4), as shown at the top of the next page. To represent (3) and (4) in the discrete form, $(k+1)T_0$ and kT_0 are rewritten as $(k+1)$ and k, respectively, resulting in (5) and (6), as shown at the top of the next page. It is worth noting here that sampling (discretization) is applied to the terms corresponding to states $\boldsymbol{x}$ and inputs $\boldsymbol{u}$ only, and not to the measurements $\boldsymbol{y}$. The sampling

$$\frac{\boldsymbol{x}((k+1)T_0) - 2\boldsymbol{x}(kT_0) + \boldsymbol{x}((k-1)T_0)}{{T_0}^2} = \bar{\boldsymbol{g}}\left[\left(\frac{\boldsymbol{x}((k+1)T_0) - \boldsymbol{x}(kT_0)}{T_0}\right), \boldsymbol{x}((k+1)T_0), \left(\frac{\boldsymbol{u}((k+1)T_0) - \boldsymbol{u}(kT_0)}{T_0}\right), \boldsymbol{u}((k+1)T_0), \boldsymbol{y}((k+1)T_0), \boldsymbol{v}((k+1)T_0)\right] \tag{3}$$

$$\boldsymbol{y}((k+1)T_0) = \boldsymbol{h}\left[\left(\frac{\boldsymbol{x}((k+1)T_0) - \boldsymbol{x}(kT_0)}{T_0}\right), \boldsymbol{x}((k+1)T_0), \left(\frac{\boldsymbol{u}((k+1)T_0) - \boldsymbol{u}(kT_0)}{T_0}\right), \boldsymbol{v}((k+1)T_0)\right] + \boldsymbol{w}((k+1)T_0) \tag{4}$$

$$\boldsymbol{x}(k+1) = \boldsymbol{g}[\boldsymbol{x}(k), \boldsymbol{x}(k-1), \boldsymbol{u}(k+1), \boldsymbol{u}(k), \boldsymbol{y}(k+1), \boldsymbol{v}(k+1)] \tag{5}$$

$$\boldsymbol{y}(k+1) = \boldsymbol{h}[\boldsymbol{x}(k+1), \boldsymbol{x}(k), \boldsymbol{u}(k+1), \boldsymbol{u}(k), \boldsymbol{v}(k+1)] + \boldsymbol{w}(k+1) \tag{6}$$

of these terms introduces discretization error but it has been adequately included in the process noise term $\boldsymbol{v}$ so that the performance of DSE is not adversely impacted [20].

In the state estimation problem, the state $\boldsymbol{x}(k+1)$ is considered to be a random variable with an estimated mean and covariance as $\hat{\boldsymbol{x}}(k+1)$ and $\boldsymbol{P}_x(k+1)$, respectively. The measurement noise denoted as $\boldsymbol{w}(k+1)$ is additive, while the process noise denoted as $\boldsymbol{v}(k+1)$ is not additive, as can be seen in (5) and (6). $\boldsymbol{v}(k+1)$ is nonlinearly related to the state and measurement. Constant covariance matrices are considered for both measurement noise $\boldsymbol{R}$ and process noise $\boldsymbol{Q}$. The problem formulation considers the process noise $\boldsymbol{v}(k+1)$ as a state and thus adds it to the state $\boldsymbol{x}(k+1)$. This addition results in augmented state random variable $\boldsymbol{\chi}(k+1) = [\boldsymbol{x}(k+1)^T, \boldsymbol{v}(k+1)^T]^T$. $\hat{\boldsymbol{\chi}}(k+1)$ and $\boldsymbol{P}_\chi(k+1)$ denote the estimated mean and covariance of $\boldsymbol{\chi}(k+1)$, respectively. Thus, (5) and (6) can be restructured as:

$$\boldsymbol{\chi}(k+1) = \boldsymbol{g}[\boldsymbol{\chi}(k), \boldsymbol{\chi}(k-1), \boldsymbol{u}(k+1), \boldsymbol{u}(k), \boldsymbol{y}(k+1), \boldsymbol{v}(k+1)] \tag{7}$$

$$\boldsymbol{y}(k+1) = \boldsymbol{h}[\boldsymbol{\chi}(k+1), \boldsymbol{\chi}(k), \boldsymbol{u}(k+1), \boldsymbol{u}(k)] + \boldsymbol{w}(k+1) \tag{8}$$

A. PROBLEM STATEMENT

With inputs given as $\hat{\boldsymbol{\chi}}(k)$, $\hat{\boldsymbol{\chi}}(k-1)$, $\boldsymbol{P}_\chi(k)$, $\boldsymbol{P}_\chi(k-1)$, $\boldsymbol{g}$, $\boldsymbol{h}$, $\boldsymbol{u}(k+1)$, $\boldsymbol{u}(k)$, $\boldsymbol{y}(k+1)$, $\boldsymbol{R}$, and, $\boldsymbol{Q}$, evaluate $\hat{\boldsymbol{\chi}}(k+1)$ and $\boldsymbol{P}_\chi(k+1)$, in a way that the state estimation algorithm is decentralized, and uses only the local end measurements (which can be easily measured using PMUs/MUs).

B. METHODOLOGY

The conceptualization of the overall methodology used for the decentralized DSE in the transmission line is presented in Figure 1. The local end is equipped with measuring infrastructure for measuring the local end voltage and current. This work uses the sampled (instantaneous) measurements of the voltage and current. The motivation to choose sampled measurements over phasors is that the phasors are updated at a lower frequency compared to sampled measurements. With a reduced update rate of phasors, the accuracy to record a transient event reduces. A sampling rate of 1.25 kHz (i.e., each sample arrives in 0.8 milliseconds) is used in this work which is capable of preserving the signal information to be used in state estimation problems. For a given measurement, white Gaussian noise is added to the true value of the measurement to model their finite accuracy. The mean of the added noise is considered as zero, while the standard deviation (SD) is taken corresponding to the respective measurement accuracy. The measurement units send the sampled measurements and their associated noise variances to the DSE block. Since this method utilizes only the local end measurements for estimation purposes, the communication requirements are easily qualified. The DSE block utilizes these sampled measurements and estimates the state vector (i.e., remote end voltage and current) using UKF in a decentralized manner. Thereafter, the estimates of the state vector could be sent to a local substation or central control center to be used in applications like monitoring, protection, and dynamic security assessment.

III. MODELLING

A. TRANSMISSION LINE MODELLING AND THE DISCRETE DIFFERENTIAL AND ALGEBRAIC EQUATIONS (DAEs)

This section presents the derivation of the discrete DAEs of a transmission line by using continuous DAEs. A single-phase π-model representation of a transmission line is presented in Figure 2. The resistance, inductance, and shunt capacitance of a transmission line are represented as R_J, L_J, and C_J, respectively. The sending and receiving end current are represented as i_J and i_j, respectively. Similarly, the sending and receiving end voltage is represented as v_J and v_j, respectively. For UKF-based DSE, the sending end currents are taken as the measurements $z = (i_A, i_B, i_C)$, while the sending end voltages are taken as the pseudo inputs $u = (v_A, v_B, v_C)$. The receiving end currents and receiving end voltages are the estimated quantities $x = (i_a, i_b, i_c, v_a, v_b, v_c)$ as presented in Figure 1.

The continuous DAEs for a transmission line model as shown in Figure 2, can be written as:

$$i_J = i_j + C_J\frac{dv_j}{dt} + C_J\frac{dv_J}{dt} \tag{9}$$

$$v_J = v_j + R_J\left[i_j + C_J\frac{dv_j}{dt}\right] + L_J\left[\frac{di_j}{dt} + C_J\frac{d^2v_j}{dt^2}\right] \tag{10}$$

where subscript J represents the sending end side and subscript j represents the receiving end side.

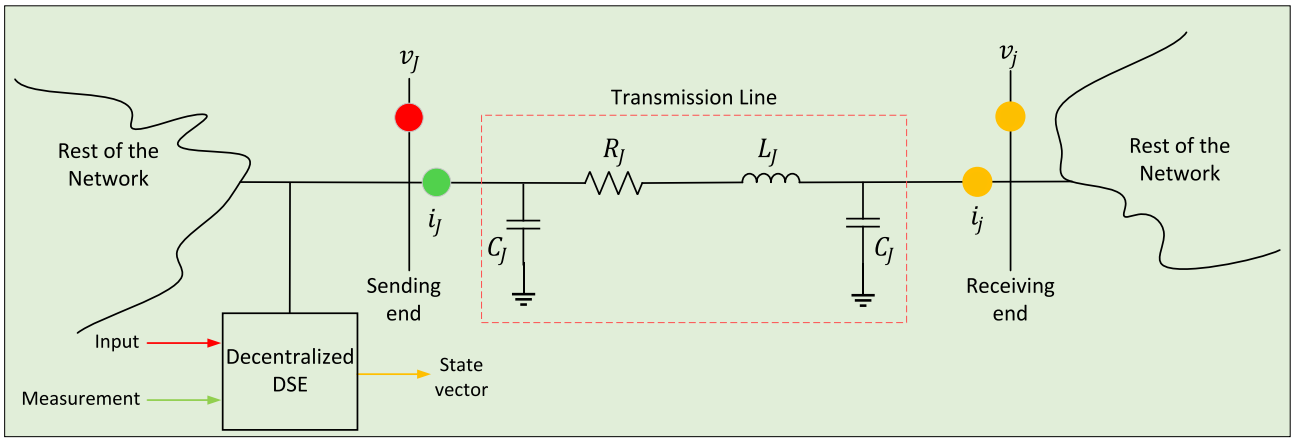

FIGURE 1. Conceptualization of the proposed methodology.

The discrete DAEs of a transmission line are obtained using the continuous DAEs and are presented in (20)−(25). Among these equations, (5) corresponds to (24) and (25), while (6) corresponds to (21).

B. UNSCENTED KALMAN FILTER

A UKF was proposed to overcome the limitations associated with an extended Kalman filter (EKF). UKF has higher accuracy and easier implementation as compared to EKF. The nonlinear transformations are used for the propagation of mean and covariance data in UKF. The basis of UKF is that the approximation of a probability distribution is simpler compared to the approximation of a nonlinear function. Based on the previous intuition, it can be implied that consistent, efficient, and unbiased estimates of a function that is going through a nonlinear transformation could be obtained using this method [3], [21], [22], [23]. It is important to mention here that the UKF variant used in this work does not suffer from the issue concerning the choice of selecting the sigma points weights in the UKF. Also, the stability index of the UKF variant used in this work is independent of the number of states and thus has better performance than the generic UKF [20].

With the application of the nonlinear transformation presented in (7) to $\boldsymbol{\chi}(k)$, the estimates of the mean and covariance of the subsequent state vector $\boldsymbol{\chi}(k+1)$ can be evaluated as explained in the following steps [3], [20]:

1) *Sigma Points Generation*: This step generates a set of points, referred to as sigma points. The sample mean and covariance of these points and $\boldsymbol{\chi}(k)$ are equal. For capturing its distribution, exactly $2n$ sigma points $\boldsymbol{\chi}_m(k)$ needs to generated, given that the dimension of $\boldsymbol{\chi}(k)$ is n, then for capturing its distribution [23]. The sigma points can be generated using the following equations:

$$\boldsymbol{\chi}_m(k) = \hat{\boldsymbol{\chi}}(k) + (\sqrt{n\boldsymbol{P}_\chi(k)})_m \quad m = 1, 2, \ldots, n \tag{11}$$

$$\boldsymbol{\chi}_m(k) = \hat{\boldsymbol{\chi}}(k) - (\sqrt{n\boldsymbol{P}_\chi(k)})_m \quad m = n+1, n+2, \ldots, 2n \tag{12}$$

where $(\sqrt{n\boldsymbol{P}_\chi(k)})_m$ is mth column of the lower triangular matrix $\sqrt{n\boldsymbol{P}_\chi(k)}$ and can be obtained through Cholesky decomposition, given as

$$n\boldsymbol{P}_\chi(k) = \left(\sqrt{n\boldsymbol{P}_\chi(k)}\right)\left(\sqrt{n\boldsymbol{P}_\chi(k)}\right)^T \tag{13}$$

2) *Predict State*: The predicted state sigma points $\boldsymbol{\chi}_m^-(k+1)$ are generated using the sigma points. The estimated mean $\hat{\boldsymbol{\chi}}^-(k+1)$ and the estimated covariance $\boldsymbol{P}_\chi^-(k+1)$ of a predicted state random variable are equal to the sample mean and sample covariance of the predicted state sigma points, respectively, whose expressions are given as:

$$\boldsymbol{\chi}_m^-(k+1) = \boldsymbol{g}[\boldsymbol{\chi}_m(k), \boldsymbol{u}(k)] \quad m = 1, 2, \ldots, 2n \tag{14}$$

$$\hat{\boldsymbol{\chi}}^-(k+1) = \frac{1}{2n}\sum_{m=1}^{2n}\boldsymbol{\chi}_m^-(k+1) \tag{15}$$

$$\boldsymbol{P}_\chi^-(k+1) = \frac{1}{2n}\sum_{m=1}^{2n}[\boldsymbol{\chi}_m^-(k+1) - \hat{\boldsymbol{\chi}}^-(k+1)] \times [\boldsymbol{\chi}_m^-(k+1) - \hat{\boldsymbol{\chi}}^-(k+1)]^T + \begin{bmatrix} \boldsymbol{Q} & \boldsymbol{0}_{s\times 3} \\ \boldsymbol{0}_{3\times s} & \boldsymbol{0}_{3\times 3} \end{bmatrix} \tag{16}$$

where s is the total number of states to be estimated.

3) *Predict Measurement*: In this step, the predicted measurement sigma points $\boldsymbol{\gamma}_m^-(k+1)$ are generated. The estimated mean $\hat{\boldsymbol{y}}^-(k+1)$ of a predicted measurement random variable is equal to the sample mean of the predicted measurement sigma points and the estimated covariance $\boldsymbol{P}_y^-(k+1)$ is equal to the sum of $\boldsymbol{R}$ and sample covariance of the predicted measurement sigma points. The estimated cross-correlation covariance between the predicted state sigma points and predicted measurement sigma points is $\boldsymbol{P}_{\chi y}^-(k+1)$. These expressions are given as:

$$\boldsymbol{\gamma}_m^-(k+1) = \boldsymbol{h}[\boldsymbol{\chi}_m^-(k+1), \boldsymbol{u}(k+1)]$$

$$m = 1, 2, \ldots, 2n \tag{17}$$

$$\hat{\boldsymbol{y}}^{-}(k+1) = \frac{1}{2n}\sum_{m=1}^{2n} \boldsymbol{\gamma}_m^{-}(k+1) \tag{18}$$

$$\boldsymbol{P}_y^{-}(k+1) = \frac{1}{2n}\sum_{m=1}^{2n}[\boldsymbol{\gamma}_m^{-}(k+1) - \hat{\boldsymbol{y}}^{-}(k+1)] \times [\boldsymbol{\gamma}_m^{-}(k+1) - \hat{\boldsymbol{y}}^{-}(k+1)]^T + \boldsymbol{P}_w \tag{19}$$

For the conversion of the continuous DAEs of a transmission line into the discrete DAEs, the following formulations are used:

$$\frac{d^2x}{dt^2} = \frac{x(k+1) - 2x(k) + x(k-1)}{T^2}, \quad \frac{dx}{dt} = \frac{x(k+1) - x(k)}{T}, \; x = x(k+1) \tag{20}$$

Applying the formulations presented in (20) to (9), leads to:

$$i_J(k+1) = i_j(k+1) + C_J\left[\frac{v_j(k+1) - v_j(k)}{T}\right] + C_J\left[\frac{v_J(k+1) - v_J(k)}{T}\right] + w(k+1) \tag{21}$$

$$i_j(k+1) = i_J(k+1) + v_j(k+1)\left[-\frac{C_J}{T}\right] + v_j(k)\left[\frac{C_J}{T}\right] + v_J(k+1)\left[-\frac{C_J}{T}\right] + v_J(k)\left[\frac{C_J}{T}\right] + w(k+1) \tag{22}$$

Restructuring (10) and applying the same formulations as presented in (20), leads to:

$$\frac{dv_j}{dt} = -\left(\frac{1}{R_J C_J}\right)v_j - \left(\frac{1}{C_J}\right)i_j + \left(\frac{1}{R_J C_J}\right)v_J - \left(\frac{L_J}{R_J C_J}\right)\frac{di_j}{dt} - \left(\frac{L_J}{R_J}\right)\frac{d^2 v_j}{dt^2}$$

$$\left[\frac{v_j(k+1) - v_j(k)}{T}\right] = -v_j(k+1)\left(\frac{1}{R_J C_J}\right) - i_j(k+1)\left(\frac{1}{C_J}\right) + v_J(k+1)\left(\frac{1}{R_J C_J}\right) - \left[\frac{i_j(k+1) - i_j(k)}{T}\right]\left(\frac{L_J}{R_J C_J}\right) - \left[\frac{v_j(k+1) - 2v_j(k) + v_j(k-1)}{T^2}\right]\left(\frac{L_J}{R_J}\right) + \upsilon(k+1)$$

$$v_j(k+1) = v_j(k)E_1 + v_j(k-1)E_2 + i_j(k)E_3 + i_j(k+1)E_4 + v_J(k+1)E_5 + \upsilon(k+1) \tag{23}$$

where,

$$E_1 = \left[\frac{C_J(TR_J + 2L_J)}{D}\right], \quad E_2 = \left[\frac{-L_J C_J}{D}\right], \; E_3 = \left[\frac{TL_J}{D}\right], \; E_4 = \left[\frac{-T(TR_J + L_J)}{D}\right], \; E_5 = \left[\frac{T^2}{D}\right],$$
$$D = [TR_J C_J + T^2 + C_J L_J].$$

Substituting $i_j(k+1)$ from (22) into (23), leads to:

$$v_j(k+1) = v_j(k)E_1 + v_j(k-1)E_2 + i_j(k)E_3 + \left[i_J(k+1) + v_j(k+1)\left(-\frac{C_J}{T}\right) + v_j(k)\left(\frac{C_J}{T}\right) + v_J(k+1)\left(-\frac{C_J}{T}\right) + v_J(k)\left(\frac{C_J}{T}\right) + w(k+1)\right]E_4 + v_J(k+1)E_5 + \upsilon(k+1)$$

$$v_j(k+1) = F_1 v_j(k) - F_1 v_j(k-1) + F_2 i_j(k) + F_3 i_J(k+1) + F_4 v_J(k) + F_5 v_J(k+1) + w(k+1) + \upsilon(k+1) \tag{24}$$

where,

$$F_1 = \left[\frac{TE_1 + E_4 C_J}{T + E_4 C_J}\right], \quad F_2 = \left[\frac{TE_3}{T + E_4 C_J}\right], \; F_3 = \left[\frac{TE_4}{T + E_4 C_J}\right], \; F_4 = \left[\frac{E_4 C_J}{T + E_4 C_J}\right], \; F_5 = \left[\frac{T}{T + E_4 C_J}\right]$$

Substituting $v_j(k+1)$ from (24) into (22), leads to:

$$i_j(k+1) = i_J(k+1) + v_j(k)\left[\frac{C_J}{T}\right] + v_J(k+1)\left[-\frac{C_J}{T}\right] + v_J(k)\left[\frac{C_J}{T}\right] + [F_1 v_j(k) - F_1 v_j(k-1) + F_2 i_j(k) + F_3 i_J(k+1) + F_4 v_J(k) + F_5 v_J(k+1) + w(k+1) + \upsilon(k+1)]\left[-\frac{C_J}{T}\right] + w(k+1)$$

$$i_j(k+1) = M_1 i_J(k+1) + M_2 v_j(k) + M_3 v_J(k+1) + M_4 v_J(k) + M_5 v_j(k-1) + M_6 i_j(k) + w(k+1) + \upsilon(k+1) \tag{25}$$

where,

$$M_1 = \left[1 - \frac{F_3 C_J}{T}\right], \quad M_2 = \left[(1-F_1)\frac{C_J}{T}\right], \; M_3 = \left[-(1+F_5)\frac{C_J}{T}\right], \; M_4 = \left[(1-F_4)\frac{C_J}{T}\right], \; M_5 = \left[F_1\frac{C_J}{T}\right],$$
$$M_6 = \left[-F_2\frac{C_J}{T}\right]$$

$$\boldsymbol{P}^-_{\chi y}(k+1) = \frac{1}{2n}\sum_{m=1}^{2n}[\boldsymbol{\chi}^-_m(k+1) - \hat{\boldsymbol{\chi}}^-(k+1)][\boldsymbol{\gamma}^-_m(k+1) - \hat{\boldsymbol{y}}^-(k+1)]^T \tag{26}$$

where $\boldsymbol{P}_w$ is the measurement noise covariance matrix.

4) *Kalman Update*: In the last step, $\hat{\boldsymbol{\chi}}(k+1)$ and $\boldsymbol{P}_\chi(k+1)$ are calculated through the standard Kalman filter [24]:

$$\begin{aligned}\boldsymbol{K}(k+1) &= \boldsymbol{P}^-_{\chi y}(k+1)[\boldsymbol{P}^-_y(k+1)]^{-1}\\ \hat{\boldsymbol{\chi}}(k+1) &= \hat{\boldsymbol{\chi}}^-(k+1) + \boldsymbol{K}(k+1)[\boldsymbol{y}(k+1) - \hat{\boldsymbol{y}}^-(k+1)]\\ \boldsymbol{P}_\chi(k+1) &= \boldsymbol{P}^-_\chi(k+1) - \boldsymbol{K}(k+1)[\boldsymbol{P}^-_{\chi y}(k+1)]^T\end{aligned} \tag{27}$$

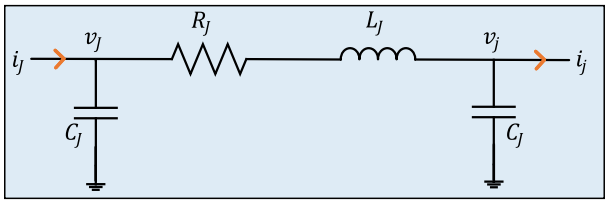

FIGURE 2. A single-phase π-model representation of a transmission line with designated variables.

C. PSEUDO INPUTS

Pseudo inputs lay the foundation for the proposed decentralized DSE method. It can be observed from (24) and (25) that the $(k+1)$th sample dynamic states and sending end current (i_J) can be expressed explicitly in terms of kth sample dynamic states and sending end voltage (v_J). This inspection suggests that if the sending end current (i_J) are considered as inputs, instead of conventional measurements, then dynamic equations of the concerned transmission line can be separated from other transmission lines in the network. Thus, the decentralized concept suggests treating one set of measurements as inputs and another set of measurements as conventional measurements. In the considered transmission line, any set of measurements (either voltages or currents) can be considered as pseudo inputs.

The consideration of sending end voltage v_J as the inputs needs to be addressed as only the measured values of v_J are available (given as v_{yA}, v_{yB}, v_{yC}), not their actual values. Since the measurements are contaminated and have their associated noises (given as v_{wA}, v_{wB}, v_{wC}), they are required to be considered. One way to consider the associated noises in the DAEs is by modelling them as input noises [25], but it requires linearization which topples the advantages associated with the unscented transformation and nonlinear filtering. Interestingly, the fact that the difference between the measured values and their associated noises is equal to the actual inputs could be utilized to include the associated noises. Using this hypothesis, the inputs can be written as:

$$v_J = v_{yJ} - v_{wJ} \tag{28}$$

Thus, $\boldsymbol{u}(k)$ and $\boldsymbol{v}(k)$ becomes pseudo input vector and pseudo-process noise vector, respectively, after the application of this hypothesis to the state function presented in (5). These vectors can be expressed as:

$$\begin{aligned}\boldsymbol{u}(k) &= [v_{yA}, v_{yB}, v_{yC}]^T\\ \boldsymbol{v}(k) &= [v_{wA}, v_{wB}, v_{wC}]^T\end{aligned} \tag{29}$$

The pseudo-process noise v_{wA}, v_{wB}, v_{wC} are white noises which have zero means and SDs as $\sigma_{v_{wA}}, \sigma_{v_{wB}}, \sigma_{v_{wC}}$. It can be deduced from this explanation that for each sample the mean $\hat{\boldsymbol{v}}(k)$ and covariance $\boldsymbol{P}_v(k)$ have a constant value and can be expressed as:

$$\begin{aligned}\hat{\boldsymbol{v}}(k) &= [\boldsymbol{0}_{3\times 1}]\\ \boldsymbol{P}_v(k) &= \boldsymbol{Q} = \text{diag}\left[\sigma^2_{v_{wA}}, \sigma^2_{v_{wB}}, \sigma^2_{v_{wC}}\right]\end{aligned} \tag{30}$$

Further, $\boldsymbol{P}_x(k)$ denotes the estimated value of the covariance of $\boldsymbol{x}(k)$, $\hat{\boldsymbol{x}}(k)$ denotes the estimated value of the mean of $\boldsymbol{x}(k)$, the cross-correlation between state $\boldsymbol{x}(k)$ and process noise $\boldsymbol{v}(k)$ is given by $\boldsymbol{P}_{xv}(k)$. $\boldsymbol{\chi}(k)$ denoting the augmentation of state $\boldsymbol{x}(k)$ and process noise $\boldsymbol{v}(k)$, can be written as:

$$\boldsymbol{\chi}(k) = [\boldsymbol{x}(k)^T, \boldsymbol{v}(k)^T]^T$$

$\hat{\boldsymbol{\chi}}(k)$ which denotes the mean of the estimates of $\boldsymbol{\chi}(k)$ and $\boldsymbol{P}_\chi(k)$ which denotes the covariance of the estimates of $\boldsymbol{\chi}(k)$ can be expressed as follows:

$$\hat{\boldsymbol{\chi}}(k) = \begin{bmatrix}\hat{\boldsymbol{x}}(k)\\ \hat{\boldsymbol{v}}(k)\end{bmatrix}; \quad \boldsymbol{P}_\chi(k) = \begin{bmatrix}\boldsymbol{P}_x(k) & \boldsymbol{P}_{xv}(k)^T\\ \boldsymbol{P}_{xv}(k) & \boldsymbol{P}_v(k)\end{bmatrix} \tag{31}$$

Similarly, the mean and covariance of measurement noise $\boldsymbol{w}(k)$ can be given as follows:

$$\begin{aligned}\hat{\boldsymbol{w}}(k) &= [\boldsymbol{0}_{3\times 1}]\\ \boldsymbol{P}_w(k) &= \boldsymbol{R} = \text{diag}\left[\sigma^2_{i_{wA}}, \sigma^2_{i_{wB}}, \sigma^2_{i_{wC}}\right]\end{aligned} \tag{32}$$

TABLE 1. Parameters and their values for the transmission line (per-phase).

Parameter	Value
Nominal voltage	345 kV
Rated frequency	60 Hz
Resistance (R)	0.037 Ω/km
Inductive Reactance ($x_L = \omega L$)	0.367 Ω/km
Susceptance ($b_C = \omega C$)	4.518 μs/km
Line length	200 km
Rated load	400 MVA
Considered load	350 MVA

D. CHOOSING ADEQUATE SAMPLING RATE OF DSE

The sampling rate of DSE is the rate at which state estimates are updated. The selection of sampling rate is one of the important parameters in UKF-based DSE of a transmission line if a detailed non-linear model is used for estimation. This is because a higher sampling rate ensures the proper capturing of any dynamic event, while at the same time, it leads to a higher discretization error as can be seen from (24). The discretization error depends mainly on the $1/(1 + E_4 C_J/T)$ term in (24), which is equal to $(R_J C_J/T + C_J L_J/T^2 + 1)$. This term becomes too large for very small T, mainly because $C_J L_J/T^2$ becomes too large. To keep this term small, $C_J L_J/T^2$ should be close to 1 which means T should be close to $\sqrt{C_J L_J}$, and not too small. T also shouldn't be too large as then UKF will fail to converge, as the dynamics will not be adequately captured. Therefore, the sampling rate (F) in the case of transmission line DSE is a trade-off between the event capturing accuracy and the discretization error, and a value of $F = 1/T \approx 1/\sqrt{C_J L_J}$ is a good balance between the two.

It should be noted that i_j has a higher discretization error as compared to v_j, because the d^2/dt^2 term first appears in v_j, which gives rise to $1/(1 + E_4 C_J/T)$ terms in (24), and introduces error in v_j. This error accumulates and becomes enhanced when v_j is again substituted in the expression of i_j, as i_j already has its own errors due to the d/dt terms (that is, the C_J/T term). Hence, making $1/(1 + E_4 C_J/T)$ small has such a significant impact on the accuracy of i_j and, therefore, on the accuracy of transmission line DSE itself.

IV. CASE STUDY

A. DESCRIPTION

The case study considered in this work is a three-phase long overhead transmission line with a nominal voltage of 345 kV. The considered parameters and their values in this simulation are presented in Table 1 and are taken from [26]. The single-line diagram of the simulation setup is presented in Figure 3.

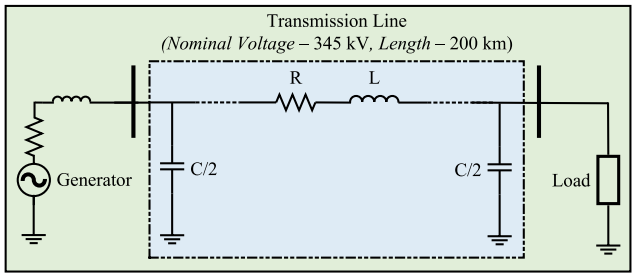

FIGURE 3. Single-line diagram of the simulation setup used.

B. SIMULATION SETUP

MATLAB Simulink (R2020b version) installed on a personal computer with Intel(R) Core(TM) i7-7700K, 4.20 GHz CPU, and 48.0 GB of RAM is used for the simulation of the case study. The simulation network consists of a long transmission line and is connected to a large generator (representing an infinite grid) at one end and a load at the other end. The transmission model is developed in Simulink and the voltages and currents of both sending and receiving ends are taken out as variables. The sending end currents are considered measurements, while the sending end voltages are considered as inputs. The receiving end currents and receiving end voltages are also taken out to be compared with their estimated values obtained from the UKF-based DSE proposed in this paper.

C. SAMPLING RATE SETUP

Based on the line parameters used in the case study, the sampling rate is taken as 0.8 milliseconds, which is close to $\sqrt{C_J L_J}$, as explained in Section III-D. A sampling rate of 0.8 milliseconds translates to a sampling frequency of 1.25 kHz.

D. OTHER PARAMETERS USED IN THE SIMULATION

1) MEASUREMENTS

In the time-domain simulation, the actual values of local end voltages and currents are sampled at 1.25 kHz ($T_0 = 800\ \mu$s), and white Gaussian noises are added to these samples to obtain the measurements [3], [20]. The motivation to consider white noise is that it is constant with respect to the frequency spectrum. Typically in the field, the measurements are acquired through the instrumentation chain which induces thermal noise (also referred to as Johnson noise) and is a form of white noise.

2) PROCESS NOISE COVARIANCE MATRIX

The process noise has the covariance matrix (in per unit (p.u.)) $\boldsymbol{Q} = \text{diag}\{6.6 \times 10^{-6}, 6.6 \times 10^{-6}, 6.6 \times 10^{-6}\}$.

3) MEASUREMENT NOISE COVARIANCE MATRIX

The measurement noise has the covariance matrix (in p.u.) $\boldsymbol{R} = \text{diag}\{6.6 \times 10^{-6}, 6.6 \times 10^{-6}, 6.6 \times 10^{-6}\}$.

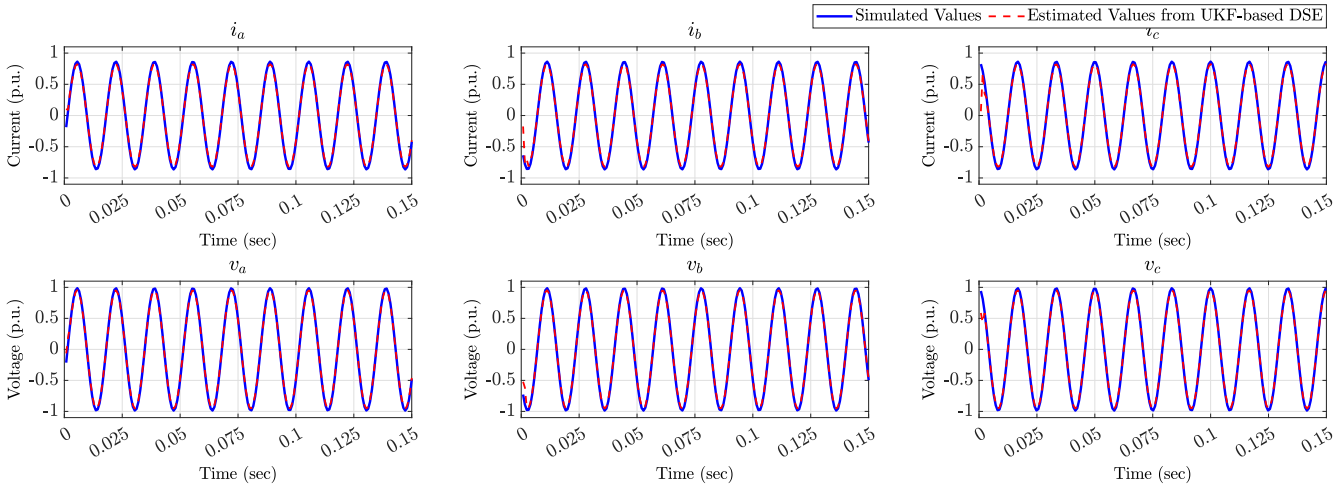

FIGURE 4. Simulated measurements and the estimated values from UKF-based DSE for the estimated quantities in case of a resistive load.

4) INITIAL VALUES

The initial values for all the variables are taken as zero. The zero initial values are an advantage as the proposed method is independent of the initial conditions and works as intended without the availability of this information.

It has to be noted that the values of matrices $\boldsymbol{R}$ and $\boldsymbol{Q}$ are calculated based on 1% Gaussian error with 99.99% confidence band (which corresponds to 0.257% SD of the noise, or 6.6×10^{-6} p.u. variance) for all the measurements.

V. RESULTS AND DISCUSSION

This section presents the results obtained from the different case studies followed by a discussion on performance. All the case studies are performed using the test setup presented in Section IV and parameters presented in Table 1. The UKF-based DSE algorithm runs simultaneously with the transmission line simulation under the given load conditions. The generated measurements are given as input to the UKF-based DSE. Each simulation is run for 0.15 seconds, while the sampling frequency of 1.25 kHz is used in the simulation. The results presented in the plots show per unit values, where the nominal voltage is 345 kV and the nominal current is calculated using the nominal voltage (345 kV) and rated load which is 400 MW.

A. WITH RESISTIVE LOAD

This subsection presents the results from UKF-based DSE when the considered load is purely resistive. The considered load is $S = 350$ MVA and as the load is purely resistive then $P = 350$ MW and $Q = 0$ MVAr. The simulated values (obtained from Simulink) along with the estimated values obtained from the UKF-based DSE are presented in Figure 4.

ESTIMATION PERFORMANCE

It can be seen from Figure 4 that the estimated values obtained from the UKF-based DSE are concurrent with the simulated values obtained from Simulink. A small mismatch can be seen at the beginning of the simulation which is due to the flat start of the guess values for the UKF-based DSE. Thus, it is evident from the results presented in Figure 4 that the UKF-based DSE accurately estimates the dynamic states of the transmission line (i.e., receiving end voltages and receiving end currents). It should be noted here that the dynamic states are estimated using the local end signals only.

B. WITH INDUCTIVE LOAD

The loading conditions in power systems are mostly inductive which could make the system response to disturbances more sluggish due to the increase in the time constant and also leads to an increased phase difference between the voltages and currents. These factors could also impact the performance of any DSE method and thus forms an interesting case to be investigated. In this regard, this subsection presents the results from UKF-based DSE when the considered load is inductive with a p.f. of 0.85. The considered load is $S = 350$ MVA and as the load is inductive with a p.f. of 0.85 then $P = 297.5$ MW and $Q = 184.4$ MVAr. The simulated values (obtained from Simulink) along with the estimated values obtained from the UKF-based DSE are presented in Figure 5.

ESTIMATION PERFORMANCE

It can be seen from Figure 5 that the estimated values obtained from the UKF-based DSE are concurrent with the simulated values obtained from Simulink with the inductive load conditions as well. A phase difference between the voltage and current could be seen in Figure 5 which is due to inductive load. Therefore, the results presented in Figure 5 confirm that the dynamic states of the transmission line (i.e., receiving end voltages and receiving end currents) are accurately estimated by the UKF-based DSE despite the phase difference between the voltages and currents due to the inductive load.

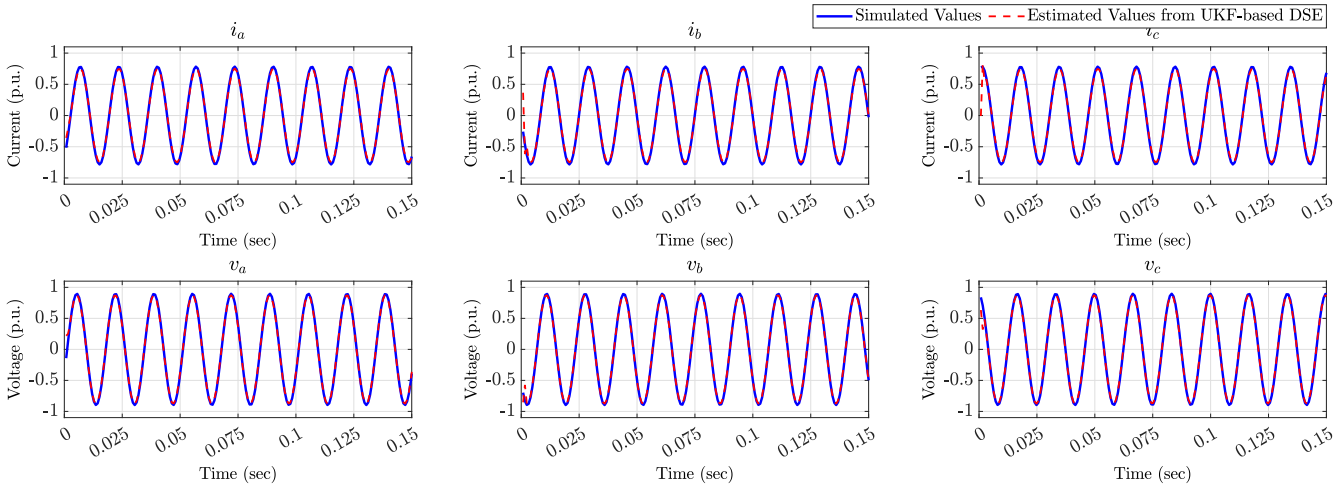

FIGURE 5. Simulated measurements and the estimated values from UKF-based DSE for the estimated quantities in case of an R-L load with pf of 0.85.

C. UNDER LOAD CHANGE CONDITIONS

Power systems mostly operate in the quasi-static state which means that the system operates at an operating point with small changes around this point. These small changes could be in the form of load changes which could adversely impact the performance of a DSE method. Therefore, in order to validate the performance of the proposed UKF-based DSE method during the load change conditions, this case study is performed. The base load (corresponding to 1 p.u.) is $S = 350$ MVA with a p.f. of 0.85, then $P = 297.5$ MW and $Q = 184.4$ MVAr. Thereafter, the load is increased by 10% to 1.1 p.u. at 0.05 seconds and subsequently decreased to 0.9 p.u. at 0.1 seconds. The variation of this load change is presented in Figure 6. The simulated values (obtained from Simulink) along with the estimated values obtained from the UKF-based DSE corresponding to this load change are presented in Figure 7.

ESTIMATION PERFORMANCE

Figure 7 shows that the estimated values obtained from the UKF-based DSE correctly follow the simulated values obtained from Simulink during the load change conditions as well. As the load increases at 0.05 seconds, correspondingly the current in all the phases increases, while the voltage in all the phases decreases as can be seen in Figure 7. The currents and voltages settle at a new steady state until another load change occurs at 0.1 seconds. This change decreases the load to 0.9 p.u. which leads to decreased current in all the phases, while the voltage increases. Interestingly, the estimated values from the UKF-based DSE match well with the simulated values obtained from Simulink even during the small transients that occurred due to steep load changes. It can be concluded from the results presented in Figure 7 and subsequent discussion that the dynamic states of the transmission line (i.e., receiving end voltages and receiving end currents) can be accurately estimated from the UKF-based DSE.

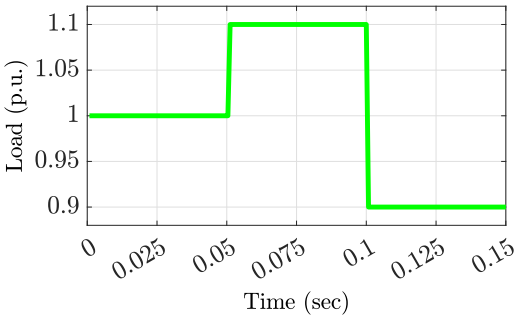

FIGURE 6. A plot showing the load change in per unit.

D. UNDER FAULT CONDITIONS

Transmission lines are also subjected to different fault conditions and satisfactory performance of a DSE method during and after the fault conditions is an important performance indicator. In this regard, this case study is performed to validate the performance of the proposed UKF-based DSE under a three-phase fault. The fault is created in the middle of the transmission line and initiated at 0.04 seconds and cleared at 0.08 seconds. A fault impedance of 1 Ω is used in the simulation. The simulated values (obtained from Simulink) along with the estimated values obtained from the UKF-based DSE corresponding to this three-phase fault are presented in Figure 8.

ESTIMATION PERFORMANCE

Figure 8 shows that before the fault is initiated (i.e., between 0 and 0.04 seconds), the estimated values obtained from the UKF-based DSE matches well with the simulated values obtained from Simulink. However, when the fault is initiated at 0.04 seconds, the simulated values go to zero because as the fault occurs in the middle of the line and is fed only from the local end, thus the remote end voltages and currents go to zero. However, the estimated values from the UKF-based DSE during the fault show a high value for both currents

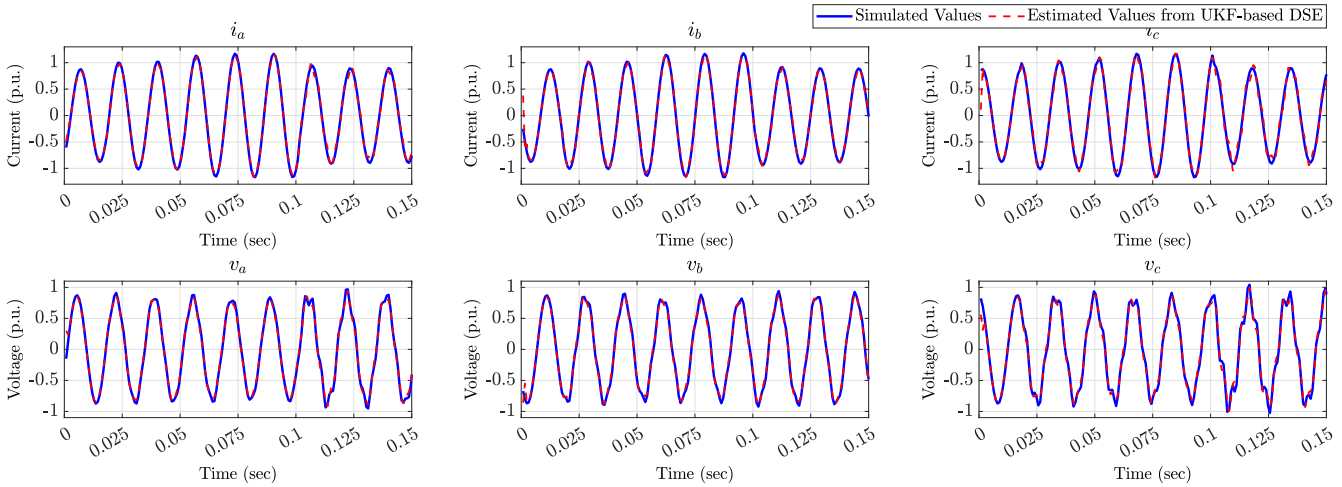

FIGURE 7. Simulated measurements and the estimated values from UKF-based DSE for the estimated quantities during load change conditions.

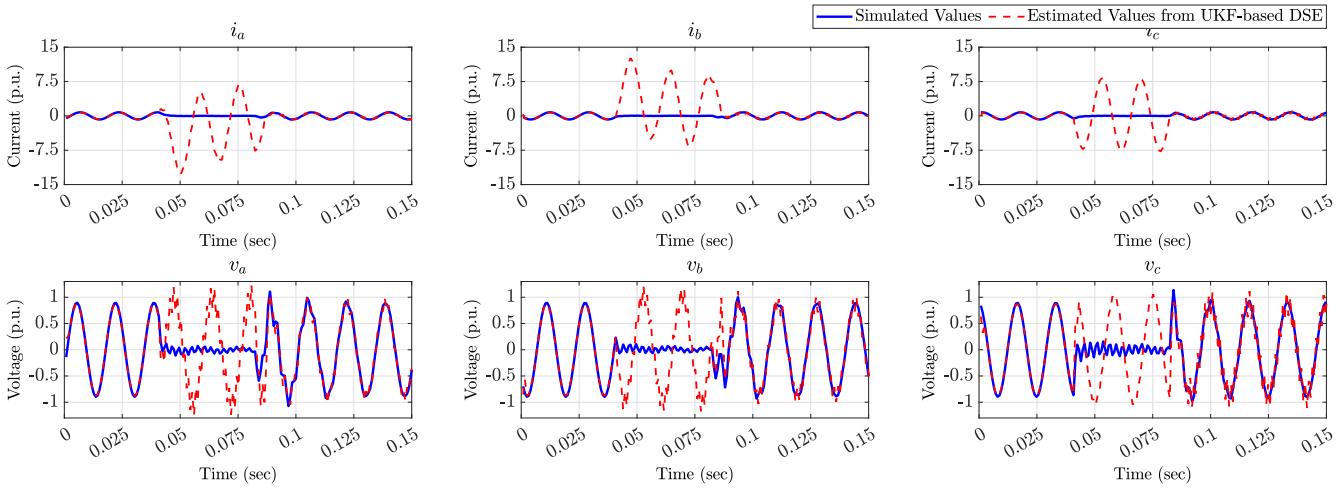

FIGURE 8. Simulated measurements and the estimated values from UKF-based DSE for the estimated quantities with a three-phase fault.

(peak value of 12 p.u.) and voltages (peak value of 1.2 p.u.) which are different from the simulated values. The main reason behind the mismatch is that the UKF-based DSE is using only the local end variables (i.e., voltages and currents) in the estimation process which go high during the fault and thus it predicts the remote end variables as high. After the fault is cleared at 0.08 seconds, the estimated values from the UKF-based DSE again match well with the simulated values.

It is interesting to note here that the performance of the proposed UKF-based DSE method during the fault is associated with the idea of the DSE-based protection scheme. This protection scheme identifies a fault based on the mismatch of simulated and estimated values during the fault. Experimental validation of one such version of the DSE-based protection scheme is presented in [7] and [15].

E. LOAD FED FROM BOTH ENDS

Transmission systems are generally connected in meshed structure and the loads are fed from sources at both ends. The investigation of the DSE method under such conditions is an interesting case study. The considered load is resistive with $S = 350$ MVA and thus $P = 350$ MW and $Q = 0$ MVAr in this case study. The simulated values (obtained from Simulink) along with the estimated values obtained from the UKF-based DSE are presented in Figure 9.

ESTIMATION PERFORMANCE

It can be seen from Figure 9 that the estimated values obtained from the UKF-based DSE are concurrent with the simulated values obtained from Simulink during the condition where the load is fed from both ends. In this case, the receiving end current in all phases is close to 0.2 p.u. as part of the load current is fed from the other end, while the receiving end voltage is close to 1 p.u. Therefore, the results presented in Figure 9 affirm that the dynamic states of the transmission line (i.e., receiving end voltages and receiving end currents) are accurately estimated by the UKF-based DSE during the condition where the load is fed from both ends.

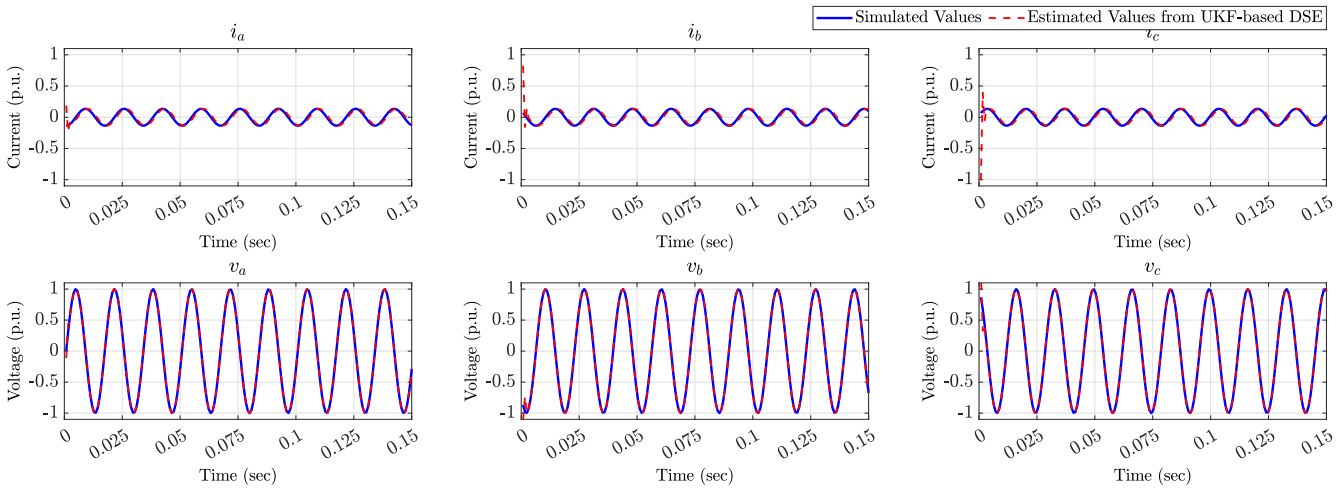

FIGURE 9. Simulated measurements and the estimated values from UKF-based DSE for the estimated quantities with the load fed from both ends.

TABLE 2. Estimation RMSE using different noise variance and type.

Type of Noise	Standard Deviation of Noise	Estimation RMSE			
		Voltage		Current	
		Mean	SD	Mean	SD
Gaussian	0.257%	2.3%	2E-5	3.2%	3E-5
	1%	3.0%	12E-5	4.1%	17E-5
	4%	8.0%	61E-5	11.0%	91E-5
Laplacian	0.257%	2.3%	2E-5	3.3%	3E-5
	1%	3.0%	14E-5	4.1%	19E-5
	4%	8.0%	78E-5	11%	113E-5

F. COMPUTATIONAL FEASIBILITY

The computational feasibility of the proposed decentralized DSE method is evaluated using the case study presented in Section IV. The sampled measurements are updated every 0.8 milliseconds (i.e., $T_0 = 0.8$ milliseconds), which means that in order to run in real-time, the method should compute the estimates in time less than 0.8 milliseconds for one set of measurements. In this regard, the average time of the proposed DSE method for obtaining the estimates of one set of measurements is calculated as 0.072 milliseconds. The configuration of the computer used in this work is given in Section IV-B, while the CPU load was close to 16%. It can be easily inferred that the proposed DSE method runs very fast and the average time for obtaining estimates for one set of measurements is much less than the measurement update time. In other words, the proposed DSE method runs in real-time along with the exclusion of linearization and approximation errors involved in the modelling and estimation method.

VI. EVALUATION OF ESTIMATION ACCURACY

A. USING DIFFERENT NOISE VARIANCE AND TYPE

Noise can have a significant impact on the performance of a state estimation method. The noises could be of different types such as Gaussian or non-Gaussian and could have different variances depending on the metering infrastructure. The noise considered in all the case studies presented in Section V is Gaussian, while the percentage error is 1%, which is close enough to today's metering infrastructure but can still be considered conservative compared to the conditions where meters are installed in the field [27], [28]. Therefore, the robustness of the proposed method is evaluated further with higher variances than the base case and as well as with Laplacian noise type (non-Gaussian).

To evaluate the robustness, the root mean square error (RMSE) associated with estimation is calculated with different error types and SDs. It shall be noted that all the RMSE calculations in Table 2 are system based and not the actual values. The first three cases consider the Gaussian noise with 0.257% (base case), 1%, and 4% as SD, while the last three cases consider the Laplacian noise with 0.257%, 1%, and 4% as SD. The results with estimation RMSE under these cases are presented in Table 2. In each case, RMSE is calculated using a Monte-Carlo-based process with the number of Monte-Carlo simulations taken as 1000. Thereafter, the Gaussian probability distribution is fitted for RMSEs obtained from each simulation. Finally, a mean value along with its SD is obtained for each case as presented in Table 2.

It can be seen from Table 2 that with Gaussian noise, for the base case with 0.257% noise SD, the mean of estimation RMSE is 2.4% and 3.3% in voltage and current, respectively. With increasing noise SD (i.e., 1% and 4%), the mean of estimation RMSE increases in both voltage and current. Interestingly, with 4% noise SD which is almost 16 times higher noise level than the base case, the mean of estimation RMSE increases only approximately 3 times. The RMSE estimation results obtained with Laplacian noise in all the cases are very close to the results obtained with the Gaussian noise as shown in Table 2. These results confirm the robust performance of the proposed method.

B. USING DIFFERENT ERROR METRICS

To further evaluate the performance of the proposed method, the most standard and widely accepted error metrics such as

TABLE 3. Estimation errors using different metrics with 0.257% noise SD.

Type of Noise	Root Mean Square Error		Maximum Absolute Error		Mean Absolute Error	
	Voltage	Current	Voltage	Current	Voltage	Current
Gaussian	2.3%	3.2%	5.0%	7.0%	2.1%	2.9%
Laplacian	2.3%	3.3%	5.4%	7.5%	2.1%	2.9%

RMSE, maximum absolute error (MaAE), and mean absolute error (MeAE) are employed for calculating the estimation accuracy. In this regard, the same case study as presented in Section IV is considered, while both Gaussian and Laplacian noise with 0.257% SD is used. The results obtained using RMSE, MaAE, and MeAE error metrics are presented in Table 3. In all the cases, error metrics (i.e., RMSE, MaAE, and MeAE) are calculated using a Monte-Carlo-based process with the number of Monte-Carlo simulations taken as 1000. Thereafter, the Gaussian probability distribution is fitted for each error metric (i.e., RMSE, MaAE, and MeAE) obtained from the simulation. Finally, a mean value is obtained as presented in Table 3.

It can be seen from Table 3 that results obtained with the two types of noises (Gaussian and Laplacian) are very close to each other. This observation once again confirms the robustness of the proposed method in connection to different types of noise and error metrics as well. Further, MaAE with Gaussian noise comes out as 5.0% and 7.0% for voltage and current, respectively. In the case of Laplacian noise, it comes out as 5.4% and 7.0% for voltage and current, respectively. MaAE signifies the maximum absolute error among all the samples during the entire simulation period and since MaAE is not very high, it is evident that the absolute error remains within a limited range. Similarly, in the case of MeAE, which signifies the mean of the absolute error obtained for all the samples in the simulation period. MeAE remains lower than the respective RMSE in both Gaussian and Laplacian noise cases. Overall, it can be concluded that the proposed DSE method performs well in terms of different error metrics, confirming its robustness.

C. WITH TRANSMISSION LINE PARAMETERS INACCURACY

Transmission line parameters could be dynamic in nature due to several factors and since the proposed DSE method uses these parameters as input, therefore it is important to study the impact of transmission line parameters variation on the estimation accuracy. The study performed in [29] mentions that transmission line parameters could vary up to 20%. Considering this range of variation, six cases have been studied in this subsection where transmission line parameters inaccuracy is considered to be $\pm 20\%$, $\pm 10\%$, and $\pm 5\%$. The same case study along with the static parameters as presented in Section IV is considered here.

The results in terms of estimation RMSE obtained with different percentages of transmission line parameters inaccuracy are presented in Table 4. In each case, RMSE is calculated using a Monte-Carlo-based process with the number of Monte-Carlo simulations taken as 100. Thereafter, the Gaussian probability distribution is fitted for RMSEs obtained from each simulation. Finally, a mean value of estimation RMSE is obtained for each case, presented in Table 4. Also, the Gaussian noise with 0.257% SD is considered in all the cases. For comparison purposes, the difference between the estimation RMSE obtained from each case and the case without any inaccuracy in transmission line parameters (base case) is also calculated and presented in Table 4. The estimation RMSEs for the base case are 2.33% and 3.27% for voltage and current, respectively.

TABLE 4. Estimation RMSE with different percentages of transmission line parameters inaccuracy.

Percentage Inaccuracy in Line Parameters	Estimation RMSE			
	Voltage	Percentage Difference from Base Case	Current	Percentage Difference from Base Case
-20%	3.75%	1.42%	4.92%	1.65%
-10%	2.72%	0.39%	3.61%	0.34%
-5%	2.41%	0.08%	3.28%	0.01%
+5%	2.50%	0.17%	3.57%	0.29%
+10%	2.87%	0.54%	4.13%	0.86%
+20%	3.99%	1.66%	5.66%	2.39%

It can be seen from Table 4 that with the increasing percentages of transmission line parameters inaccuracy, the estimation RMSE is also increasing and, hence, have a higher difference from the base case. This observation shows a proportional relationship between the inaccuracy of the transmission line parameters and the estimation accuracy. However, it is interesting to see that even when the transmission line parameters inaccuracy goes high even up to $+20\%$ and -20%, the estimation RMSE increases only by 2.39% and 1.65%, respectively. This increase in estimation RMSE could be considered as non-substantial compared to the case when noise SD is 4% leading to estimation RMSE of 8.0% and 11.0% in voltage and current, respectively. Thus, the obtained results confirm the robustness of the proposed DSE method against the transmission line parameters inaccuracy.

VII. CONCLUSION

The paper concludes that the performance of the proposed decentralized DSE method for estimating the dynamic states of a transmission line in real-time has been satisfactory. The proposition of the method preserves the nonlinearity

in the transmission line modelling. The method works in a decentralized manner which is achieved by treating one set of measured quantities as pseudo inputs. The feasibility of the method is evaluated by carrying out various case studies with resistive load, inductive load, load change, fault conditions, and load fed from both ends. Further, the robustness is validated by performing case studies with reasonably-high noise levels and considering transmission line parameters inaccuracy. The results obtained from these case studies highlight the intended performance of the proposed method in terms of accuracy, speed, and feasibility over other existing methods. The work presented in this paper has helped identify new research directions concerning the further development of the unscented Kalman filter-based DSE method for transmission lines. These directions include (i) exploring the performance of the proposed method using the distributed model of transmission line for cases when the length of a transmission line is more than 200 km, and (ii) applying the proposed decentralized DSE method to transmission line protection.

REFERENCES

[1] J. Zhao, M. Netto, Z. Huang, S. S. Yu, A. Gómez-Expósito, S. Wang, I. Kamwa, S. Akhlaghi, L. Mili, V. Terzija, A. P. S. Meliopoulos, B. Pal, A. K. Singh, A. Abur, T. Bi, and A. Rouhani, "Roles of dynamic state estimation in power system modeling, monitoring and operation," *IEEE Trans. Power Syst.*, vol. 36, no. 3, pp. 2462–2472, May 2021.

[2] Y. Liu, A. P. S. Meliopoulos, R. Fan, L. Sun, and Z. Tan, "Dynamic state estimation based protection on series compensated transmission lines," *IEEE Trans. Power Del.*, vol. 32, no. 5, pp. 2199–2209, Oct. 2017.

[3] A. K. Singh and B. C. Pal, "Decentralized dynamic state estimation in power systems using unscented transformation," *IEEE Trans. Power Syst.*, vol. 29, no. 2, pp. 794–804, Mar. 2014.

[4] Y. Xu, Z. Y. Dong, J. H. Zhao, P. Zhang, and K. P. Wong, "A reliable intelligent system for real-time dynamic security assessment of power systems," *IEEE Trans. Power Syst.*, vol. 27, no. 3, pp. 1253–1263, Aug. 2012.

[5] Y. Lin and X. Wang, "A data-driven scheme based on sparse projection oblique randomer forests for real-time dynamic security assessment," *IEEE Access*, vol. 10, pp. 79469–79479, 2022.

[6] Y. Liu, A. K. Singh, J. Zhao, A. P. S. Meliopoulos, B. Pal, M. A. b. M. Ariff, T. Van Cutsem, M. Glavic, Z. Huang, I. Kamwa, L. Mili, A. S. Mir, A. Taha, V. Terzija, and S. Yu, "Dynamic state estimation for power system control and protection," *IEEE Trans. Power Syst.*, vol. 36, no. 6, pp. 5909–5921, Nov. 2021.

[7] A. Srivastava, L. A. Tuan, D. Steen, O. Carlson, O. Mansour, and D. Bijwaard, "Transmission line protection using dynamic state estimation and advanced sensors: Experimental validation," *IEEE Trans. Power Del.*, vol. 38, no. 1, pp. 162–176, Feb. 2023.

[8] B. Wang, Y. Liu, K. Yue, D. Lu, and J. Zhao, "Improved dynamic state estimation based protection on transmission lines in MMC-HVDC grids," *IEEE Trans. Power Del.*, vol. 37, no. 5, pp. 3567–3581, Oct. 2022.

[9] A. P. S. Meliopoulos, G. J. Cokkinides, P. Myrda, Y. Liu, R. Fan, L. Sun, R. Huang, and Z. Tan, "Dynamic state estimation-based protection: Status and promise," *IEEE Trans. Power Del.*, vol. 32, no. 1, pp. 320–330, Feb. 2017.

[10] Y. Liu, A. P. Meliopoulos, L. Sun, and R. Fan, "Dynamic state estimation based protection of mutually coupled transmission lines," *CSEE J. Power Energy Syst.*, vol. 2, no. 4, pp. 6–14, Dec. 2016.

[11] Y. Liu, A. P. S. Meliopoulos, Z. Tan, L. Sun, and R. Fan, "Dynamic state estimation-based fault locating on transmission lines," *IET Gener., Transmiss. Distrib.*, vol. 11, no. 17, pp. 4184–4192, Nov. 2017.

[12] Y. Xing, Y. Liu, B. Wang, L. Yi, and X. He, "Physics-informed data-driven transmission line fault location based on dynamic state estimation," in *Proc. IEEE Power Energy Soc. Gen. Meeting (PESGM)*, Jul. 2022, pp. 1–5.

[13] B. Wang, Y. Liu, D. Lu, K. Yue, and R. Fan, "Transmission line fault location in MMC-HVDC grids based on dynamic state estimation and gradient descent," *IEEE Trans. Power Del.*, vol. 36, no. 3, pp. 1714–1725, Jun. 2021.

[14] B. Wang, Y. Liu, D. Lu, K. Yue, and Y. Nie, "Unsynchronized parameter-free fault location for two or three terminal double-circuit transmission lines sharing the same tower via unscented Kalman filter," *IEEE Trans. Power Del.*, vol. 38, no. 3, pp. 1731–1746, Jun. 2023.

[15] A. Srivastava, L. A. Tuan, D. Steen, O. Carlson, O. Mansour, and D. Bijwaard, "Dynamic state estimation based transmission line protection scheme: Performance evaluation with different fault types and conditions," *Int. J. Electr. Power Energy Syst.*, vol. 148, Jun. 2023, Art. no. 108994.

[16] Shalini, S. R. Samantaray, and A. Sharma, "Enhancing performance of wide-area back-up protection scheme using PMU assisted dynamic state estimator," *IEEE Trans. Smart Grid*, vol. 10, no. 5, pp. 5066–5074, Sep. 2019.

[17] J. Xie, A. P. S. Meliopoulos, and B. Xie, "Transmission line fault classification based on dynamic state estimation and support vector machine," in *Proc. North Amer. Power Symp. (NAPS)*, Sep. 2018, pp. 1–5.

[18] R. Fan, Y. Liu, R. Huang, R. Diao, and S. Wang, "Precise fault location on transmission lines using ensemble Kalman filter," *IEEE Trans. Power Del.*, vol. 33, no. 6, pp. 3252–3255, Dec. 2018.

[19] A. Srivastava, "Operation, monitoring, and protection of future power systems: Advanced congestion forecast and dynamic state estimation applications," Ph.D. dissertation, Division Electr. Power Eng., Dept. Elect. Eng., Chalmers Univ. Technol., Gothenburg, Sweden, 2022.

[20] A. K. Singh and B. Pal, *Dynamic Estimation and Control of Power Systems*. New York, NY, USA: Academic Press, 2018.

[21] S. J. Julier and J. K. Uhlmann, "New extension of the Kalman filter to nonlinear systems," *Proc. SPIE*, vol. 3068, pp. 182–193, Jul. 1997.

[22] S. J. Julier and J. K. Uhlmann, "Unscented filtering and nonlinear estimation," *Proc. IEEE*, vol. 92, no. 3, pp. 401–422, Mar. 2004.

[23] J. K. Uhlmann, "Simultaneous map building and localization for real time applications," Transfer thesis, Univ. Oxford, Oxford, U.K., 1994.

[24] R. E. Kalman, "A new approach to linear filtering and prediction problems," *J. Basic Eng.*, vol. 82, no. 1, pp. 35–45, Mar. 1960.

[25] I. Markovsky and B. De Moor, "Linear dynamic filtering with noisy input and output," *Automatica*, vol. 41, no. 1, pp. 167–171, Jan. 2005.

[26] P. S. Kundur and O. P. Malik, *Power System Stability and Control*. New York, NY, USA: McGraw-Hill, 2022.

[27] *IEEE Standard Requirements for Instrument Transformers*, IEEE Standard C57.13-2008, Jul. 2008, pp. C1–C82.

[28] *IEC Standard for Instrument Transformers*, IEC Standard 60044, 2003.

[29] D. Ritzmann, P. S. Wright, W. Holderbaum, and B. Potter, "A method for accurate transmission line impedance parameter estimation," *IEEE Trans. Instrum. Meas.*, vol. 65, no. 10, pp. 2204–2213, Oct. 2016.

ANKUR SRIVASTAVA (Member, IEEE) received the M.Tech. degree from the National Institute of Technology, Warangal, Telangana, India, in 2015, and the Ph.D. degree from the Chalmers University of Technology, Gothenburg, Sweden, in 2022, all in Electrical Engineering. He has been a Postdoctoral Researcher with the University of Connecticut, USA, since January 2023. Previously, he was a Graduate Engineer with SMS India Pvt. Ltd., India, from 2011 to 2012, and a Research Associate with the Department of Electrical Engineering, Indian Institute of Technology, Kanpur, India, from 2016 to 2017. His research interests include power system state estimation, power system protection, cyber-physical security in power systems, and renewables integration in distribution systems. He is a member of the IEEE Working Group on Power System State Estimation and IEEE Task Force on State Estimation for Integrated Energy Systems, the Development of Standard Test Cases for Power System State Estimation, and Behind-the-Meter Distributed Energy Resources: Estimation, Uncertainty Quantification, and Control.

ABHINAV KUMAR SINGH (Member, IEEE) received the B.Tech. degree from the Indian Institute of Technology Delhi, India, in 2010, and the Ph.D. degree from the Imperial College London, U.K., in 2015, all in Electrical Engineering. He is currently a Lecturer in power systems with the School of Electronics and Computer Science, University of Southampton. His research interests include real-time estimation and control of future energy networks. He won the IEEE PES Working Group Recognition Award, in 2016 and 2022, for his contributions to IEEE PES Task Force on Benchmark Systems for Small Signal Stability Analysis and Control, and IEEE PES Task Force on Dynamic State and Parameter Estimation, respectively.

LE ANH TUAN (Member, IEEE) received the B.Sc. degree in Power Systems from the Hanoi University of Technology, Vietnam, in 1995, the M.Sc. degree in Energy Economics from the Asian Institute of Technology, Bangkok, Thailand, in 1997, and the Ph.D. degree in Power Systems from the Chalmers University of Technology, Gothenburg, Sweden, in 2004. He is currently an Associate Professor with the Division of Electric Power Engineering, Department of Electrical Engineering, Chalmers University of Technology. His current research interests include modeling, optimization, control, protection of integrated energy systems, active distribution networks with the high level of renewables and energy storage, wide-area monitoring and control of large power transmission systems, machine learning applications to power systems, and modeling and design of energy and ancillary service markets.

DAVID STEEN (Member, IEEE) received the M.Sc. and Ph.D. degrees in Electrical Engineering from the Chalmers University of Technology, Gothenburg, Sweden, in 2008 and 2014, respectively. He is currently a Researcher with the Department of Electrical Engineering, Chalmers University of Technology. His research interests include modeling and control of integrated energy systems and distributed energy resources, such as solar PV, wind power, electric vehicles, and energy storage.

ABDUL SALEEM MIR (Member, IEEE) received the B.Tech. degree (Hons.) in Electrical Engineering from the National Institute of Technology, Srinagar, Jammu and Kashmir, in 2014, and the Ph.D. degree in Electrical Engineering from the Indian Institute of Technology Delhi, India, in 2020. He is currently an Assistant Professor with the Department of Electrical Engineering, Indian Institute of Technology Roorkee, India. From October 2020 to December 2021, he was a Research Fellow with the University of Southampton and the Imperial College London as collaboration institute. His research interests include dynamic state estimation and control, power system dynamics, and the modeling/control of renewable energy systems. He is a member of the IEEE PES Task Force on Dynamic State and Parameter Estimation and IEEE PES Task Force on Standard Test Cases for Power System State Estimation. He received the IEEE PES Working Group Member Recognition Award, in 2022, for his contributions to IEEE PES TF on Dynamic State and Parameter Estimation.